RSC Advances

PAPER

View Article Online
View Journal | View Issue

Cite this: *RSC Adv.*, 2017, **7**, 49091

Investigation of the hydrothermal aging of an Mn-based mullite $SmMn_2O_5$ catalyst of NO oxidation

Lina Xue,[a] Ka Xiong,[b] Haijun Chen,*[a] Kyeongjae Cho[c] and Weichao Wang[ac]

Hydrothermal aging tests are important to carry out when evaluating the hydrothermal durability of heterogeneous catalysts in vehicle exhaust emission. Here, we explored the effect of aging on an efficient Mn-based mullite catalyst ($SmMn_2O_5$) of NO oxidation. The mullite catalyst was prepared *via* the hydrothermal method and was subsequently aged in air with a 10% H_2O stream at 750 °C for 16 hours. The fresh and aged catalysts were structurally characterized using Powder X-ray diffraction(XRD), Raman, X-ray photoelectron spectroscopy (XPS), scanning electron microscope (SEM), high resolution-transmission electron microscope (HR-TEM), Brunauer–Emmett–Teller (BET) and temperature programmed desorption (TPD). For the performance evaluations, the samples were placed into a U-shape reactor furnace, and NO and NO_2 concentrations were *in situ* recorded with an NO_x analyzer. In contrast to fresh mullite, the aged sample showed a 25 °C higher light-off temperature and 11% conversion loss at its maximum conversion temperature of 300 °C. O_2-TPD of the aged sample displayed a large decrease of the desorption area, consistent with an ~3-fold loss of the BET specific surface area. Moreover, HRTEM, XPS and Raman spectroscopy results together indicated that a small portion of the mullite decomposed into perovskite $SmMnO_3$ and Mn_2O_3, which further reduced the total quantity of Mn active sites. The reduction of the BET surface area and mullite decomposition together caused the decrease of the catalytic performance. We therefore expect maintaining the specific surface area to be important for preventing the loss of catalytic performance during the hydrothermal aging process.

Received 22nd August 2017
Accepted 9th October 2017

DOI: 10.1039/c7ra09306c

rsc.li/rsc-advances

Introduction

NO_x is a highly damaging pollutant, and leads to respiratory stimulation, photochemical smog, acid rain, and harm to crops.[1–3] Ammonia selective catalytic reduction (NH_3-SCR) ($2NH_3 + NO + NO_2 \rightarrow 2N_2 + 3H_2O$) is considered to be effective at removing NO_x. To achieve a high SCR efficiency, an NO-to-NO_2 molar ratio of 1 : 1 is required.[4,5] However, in practice in diesel vehicles, after use of diesel oxidation catalysis (DOC) and a diesel particle filter (DPF) in the post-treatment system, 90% of NO_x is NO. Therefore, to achieve the faster SCR reaction, some of the NO has to be oxidized into NO_2.

Precious metals such as Pt, Pd, Au have been reported to be effective at catalyzing NO oxidation. However, their high cost and low abundance hinder their wide applications in SCR.[6,7] Therefore, the relatively low-cost zeolites and metal oxides have recently been sought as replacements for the precious metals. For instance, Kim synthesized a $La_{1-x}Sr_xCoO_3$ perovskite able to catalyze NO oxidation as well as can Pt.[8] Also, the V–Ti–W system is one of the widely used catalysts, but V^{5+} is poisonous to living beings.[2,9,10] Moreover, this system is known to exhibit poor hydrothermal performance and sulfur poisoning. Zeolite-like Cu-SSZ-13 and SAPO-34 are commercially ready to replace the V–Ti–W system. However, these zeolite systems also have the hydrothermal aging and sulfur poisoning problem.[11] For metal-doped zeolites, such as Ag-SAPO-34 and Cu-ZSM-5, the hydrothermal issue is still problematic.[12,13] It is thus important to study the hydrothermal aging mechanism systemically in such a way that new insights would be gained to suppress the aging-induced failure.

In 2012, Wang *et al.*[5] reported a mullite catalyst with remarkable catalytic performance towards NO oxidation. For this specific catalyst, octahedral and pyramidal crystal fields coexist, which makes this structure have partial characteristics of both zeolites and common oxides like Al_2O_3 and SiO_2. Two types of Mn atoms in mullite might both contribute to the NO oxidation, ensuring the high catalytic behavior. In this work, we used the hydrothermal method to synthesize the pure phase of nanocrystal mullite, with a crystal diameter of ~50 nm, and which displayed a light-off temperature as low as 192 °C. Hydrothermally aging the sample in air with 10% H_2O at 750 °C for 16 hours resulted in a three-fold decrease in its BET surface

[a]*Department of Electronics, Nankai University, Tianjin 370001, China. E-mail: chenhj@nankai.edu.cn*

[b]*Dongguan Innovative New Materials Co. Ltd, Dongguan 523000, China*

[c]*Department of Materials Science & Engineering, The University of Texas at Dallas, Richardson, TX 75252, USA*

area. Meanwhile, combining high resolution-transmission electron microscope (HR-TEM), X-ray photoelectron spectroscopy (XPS) and Raman spectroscopy showed a small portion of mullite to have been decomposed into perovskite $SmMnO_3$ and Mn_2O_3, which also contributed to the catalytic reduction. These findings helped us clarify the physics of how the hydrothermal process reduces the catalytic performance of mullite oxide.

Experiment

Sample preparation

A fresh pure phase of mullite $SmMn_2O_5$ was synthesized *via* hydrothermal methods. Precursors $Sm(NO_3)\cdot 6H_2O$, $Mn(CH_3CO_2)_2\cdot 4H_2O$ and $KMnO_4$ (all 99.98%, Aladdin) were added into 25 ml deionized water simultaneously in a molar ratio of 5 : 7 : 3, and then stirred for 30 minutes. 5.3 ml NaOH (99.98%, Aladdin) at a concentration of 5 M was added slowly to this mixture, which was then stirred for 10 more minutes. After the resulting solution was stable, it was transferred to a 100 ml stainless steel Teflon-lined autoclave, and filled 60% of the autoclave capacity. The resulting solution was hydrothermally aged at 200 °C for 12 hours. The autoclave was cooled down to room temperature, and the product was then filtered and washed 3–5 times with deionized water and 1% HNO_3. Finally, the precipitant was dried at 100 °C for 4 hours to produce a powder.

To examine the catalytic performance of this product, the powder while still fresh was compressed into a pellet, which was then crushed and sieved with an 80–100 mesh. To obtain the aged sample, a mass of ~150 mg of the sieved sample was aged in a column-type quartz tube reactor (HUASI, FIJ-2020) at 750 °C with 10% H_2O/air for 16 h.

Catalytic activity test

A mass of 100 mg of each of fresh and aged sieved $SmMn_2O_5$ samples were put into a quartz tube with packed quartz wool to keep it in place. The sample tube was then transferred into a reactor furnace (Altamira catalyst characterization system, AMI-300) and flushed continuously with 450 ppm NO and 10% O_2 in N_2 at a total flow rate of 200 sccm. The furnace was ramped at 10 °C min^{-1} to 400 °C starting from 50 °C and then cooled back to ~50 °C for another cycle. The NO concentrations were recorded with an NO_x analyzer (EcoPhysics, CLD822CMh) with an uncertainty of 0.25 ppm.

Structural characterization

Powder X-ray diffraction (XRD) measurements were taken on a Rigaku, Ultima IV powder X-ray diffractometer with Cu Kα radiation. Data were collected with 2θ ranging from 20° to 70° with a step size of 8° min^{-1}. Raman spectra were collected under a Raman microscope (Renishaw) using a 514 nm-wavelength laser at 50 mW. X-ray photoelectron spectroscopy (XPS) measurements were taken on a Thermo Escalab 250Xi spectrometer equipped with an Al Kα X-ray source. scanning electron microscope (SEM) was conducted on a ZEISS-SIGMA 500 instrument, which was able to resolve mullite crystal particles with diameters as small as ~1.6 nm. Particle size was obtained by using a ZETAPALS/BI-200SM laser particle size analyzer. The transmission electron microscope (TEM) analysis was performed with a JEOL, JEM-2010FEF microscope operated at 200 kV, which yielded a resolution of 0.1 nm in scanning transmission electron microscopy mode (STEM).

Brunauer–Emmett–Teller (BET) surface areas of the fresh and aged samples (400 mg) were measured with a 3H-2000 analyzer (BeiShiDe Instrument Technology).

Temperature programmed desorption (TPD) experiments were carried out in a quartz flow microreactor on a chemisorption analyzer (Altamira catalyst characterization system, AMI-300) equipped with a thermal conductivity detector (TCD). A mass of 50 mg of the catalyst was treated at 600 °C for 60 min in N_2 with a flow of 40 ml min^{-1}, and then the catalyst was cooled to room temperature, and then kept for 2 h at 50 °C to adsorb O_2. Finally, the sample was heated to 500 °C at a rate of 10 °C min^{-1}. The O_2 signals were detected by TCD at the outlets.

Results and discussion

Mullite $SmMn_2O_5$ containing two types of crystal fields, *i.e.*, octahedral and pyramidal, shows remarkable catalytic activity towards NO_x oxidation.[5] However, hydrothermal aging diminishes this advantage of the mullite as an effective catalyst. Determining the mechanism of this decrease in catalytic activity could help one devise strategies to reduce the catalytic performance loss. Here, structural characterization using XRD was first carried out to examine the phase change before and after the hydrothermal treatment, as displayed in Fig. 1. For the fresh sample, only the orthorhombic structure of $SmMn_2O_5$ was observed. After aging the sample, new peaks appeared at 33°, 41° and 48°. Comparing the results with the standard JCPDS database suggested that these new peaks resulted from either Mn_2O_3 (33°, 41°) or $SmMnO_3$ (48°)[14,15] due to the peak overlapping. In order to differentiate these two phases, more phase

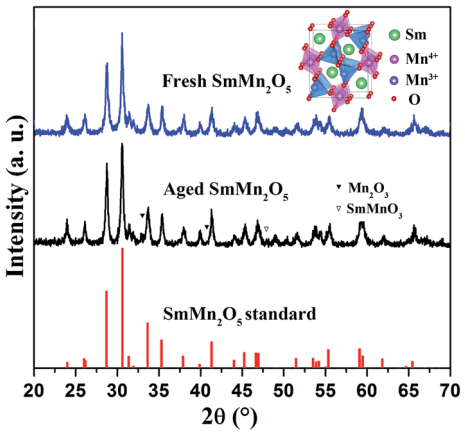

Fig. 1 XRD patterns of the fresh (blue) and aged (black) $SmMn_2O_5$ samples, as well as of standard mullite. Inset shows the two unit cells of mullite, with green, pink, and red representing the Sm, Mn and O atoms, respectively.

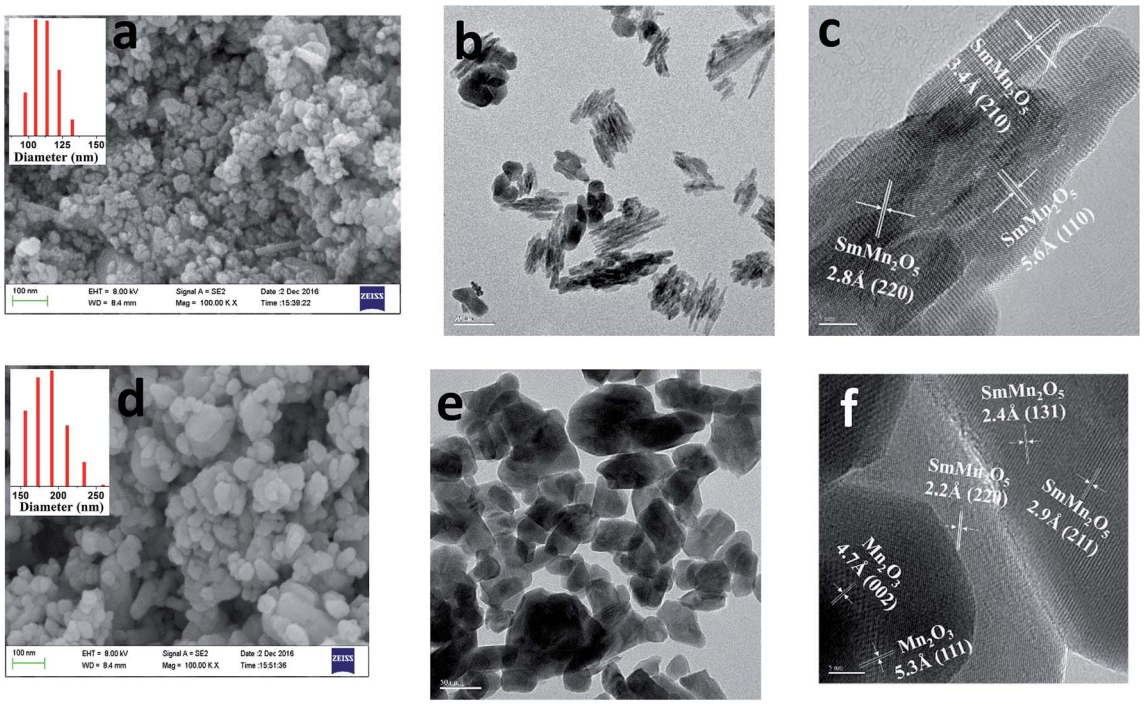

Fig. 2 (a, d) SEM images of (a) the fresh and (d) aged $SmMn_2O_5$ samples, with the insets showing the particle distributions. (b, c, e, f) HT-TEM images of the (b, c) fresh and (e, f) aged mullite samples.

characterizations and composition analyses were carried out, as described below.

TEM and SEM were subsequently utilized to assist in identifying the new phases and morphologies of the fresh and aged samples. As shown in Fig. 2a, the SEM results of the fresh sample indicated its average particle diameter to be between 100 and 130 nm. HRTEM images of the fresh sample showed these particles to be composed of nanorods (Fig. 2b) and to have a (110) surface facet with a spacing of 5.81 Å (Fig. 2c). After aging the sample at 750 °C for 16 h, the particles tended to aggregate and the particle size increased to ~200 nm (Fig. 2d). The rod-shaped particles merged to form sphere-shaped particles (Fig. 2e). More importantly, based on the surface facet spacing, a new Mn_2O_3 phase was found (Fig. 2f). As a small portion of Mn in mullite transformed into Mn_2O_3, it would be straightforward to check the status of Sm.

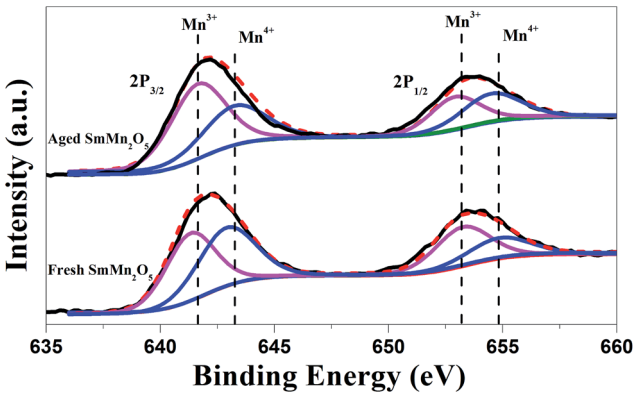

Fig. 3 XPS spectra before and after hydrothermal aging of $SmMn_2O_5$.

$SmMn_2O_5$, when subjected to phase hydrothermal aging, has been reported by A. M. Yankin *et al.*[16] to decompose into $SmMnO_3$ and MnO_x ($2SmMn_2O_5 \xrightarrow{\Delta} 2SmMnO_3 + Mn_2O_3 + O_2(g)$).

In order to check the new phase, we took XPS measurements of the sample (Fig. 3). Before the aging, the ratio of Mn^{3+} : Mn^{4+}

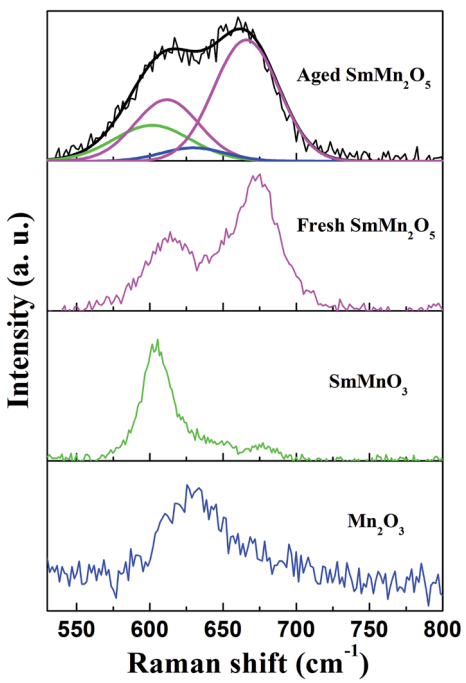

Fig. 4 Raman spectra of the fresh and aged $SmMn_2O_5$ samples, as well as of $SmMnO_3$ and Mn_2O_3.

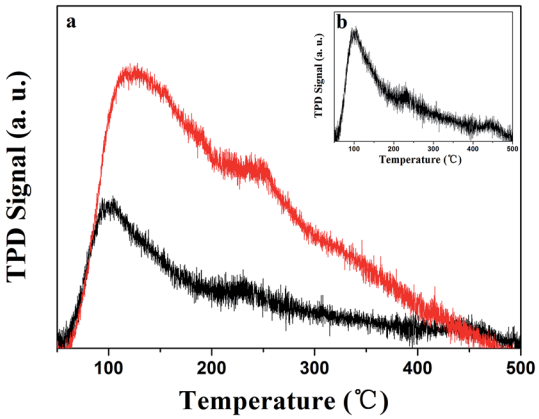

Fig. 5 O_2-TPD of (a) the fresh (red) and aged (black) $SmMn_2O_5$. (b) Inset shows that from the aged $SmMn_2O_5$.

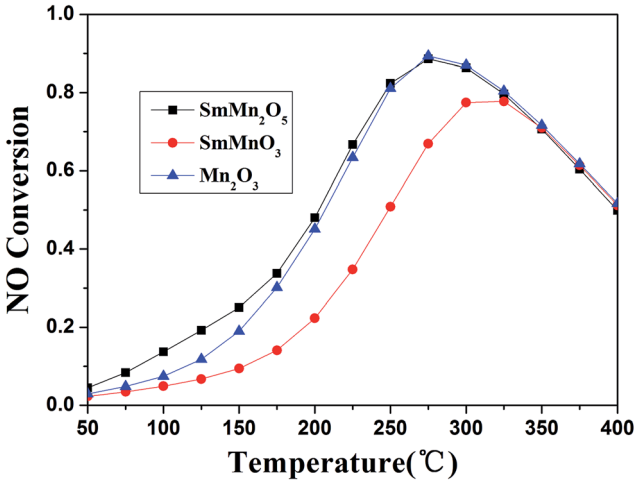

Fig. 7 NO conversion on $SmMn_2O_5$, $SmMnO_3$, and Mn_2O_3.

was indicated to be close to 1 : 1, consistent with our previous work.[17,18] After the aging, due to the occurrence of the new Mn_2O_3 phase, the relative amount of Mn^{3+} increased (Mn^{3+} : Mn^{4+} ≈ 5 : 3), which validated the TEM findings.

Furthermore, we acquired Raman spectra of the fresh and aged $SmMn_2O_5$ samples, as well as of $SmMnO_3$ and Mn_2O_3, with the wavenumbers of each of the spectra ranging from 525 to 800 cm^{-1} (Fig. 4). Peaks at ~613 cm^{-1} and ~673 cm^{-1} acquired from the fresh sample were ascribed to the Mn–O stretching vibrations.[19] Aging the sample yielded shoulders at 604 cm^{-1}, 630 cm^{-1}, which indicated the occurrence of the new phases. In order to differentiate the new phases, we fit the XPS spectrum of the aged sample with four curves as shown in Fig. 3. The peak at 604 cm^{-1} may have resulted from the Mn–O vibrations of octahedral MnO_6 of the orthorhombic perovskite (*Pnma*).[20] The peak at 630 cm^{-1} originated from the symmetric stretching of the high-pressure Mn_2O_3 phase.[21,22]

Together, the XRD, SEM, TEM, XPS and Raman spectra analyses of the fresh sample indicated the presence of only pure mullite phase. After aging the sample, the rod-shaped particles of the fresh sample tended to grow larger and meanwhile a small portion of mullite converted into Mn_2O_3 and perovskite $SmMnO_3$. This finding was consistent with the observations reported by A. M. Yankin *et al.*[16]

Aging the sample, in addition to having produced the new phase, was also expected to change the specific surface area and hence the catalytic performance.[23] In principle, this surface area would be expected to influence the gas desorption properties. Here, we combined a study of BET surface area and O_2-TPD to compare the quantity of active sites before and after hydrothermal aging. O_2-TPD experiments were carried out to gain insight into the nature of the surface oxygen species possibly involved in the redox reactions. The areas of the peaks of the

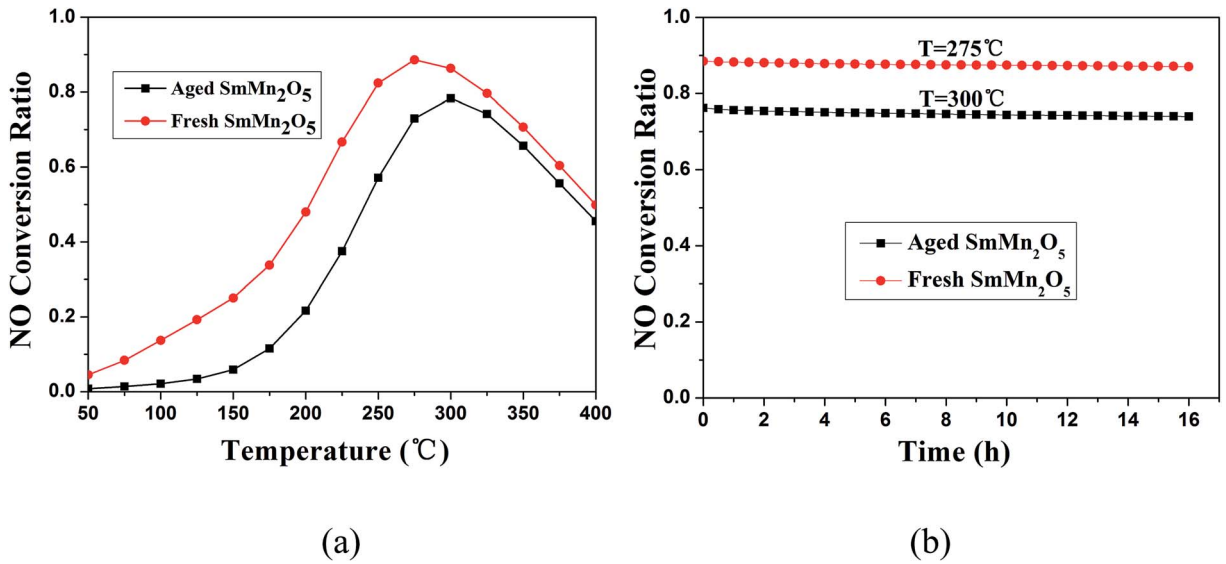

Fig. 6 (a) NO conversions in the presence of fresh or aged $SmMn_2O_5$. (b) The NO oxidation profiles of the fresh and aged $SmMn_2O_5$ samples at 275 °C and 300 °C, respectively.

Table 1 BET specific surface areas and the integrated O_2-TPD peaks of the fresh and aged $SmMn_2O_5$

	Fresh $SmMn_2O_5$	Aged $SmMn_2O_5$	$SmMnO_3$	Mn_2O_3	Ratio (fresh/aged)
BET (m^2 g^{-1})	58.84	19.19	20.62	21.88	3.11
O_2-TPD	786	319	N/A	N/A	2.46

fresh and aged $SmMn_2O_5$ species at different temperatures can be directly related to the oxidation state of the catalyst and to the oxygen coordination number.[24]

For both fresh and aged samples, three peaks were observed, as shown in Fig. 5. At low temperatures, physically adsorbed oxygen predominated on the surface.[25] Increasing the temperature yielded the second peak, which was related to O_2^- (and/or O^-) species formed by the adsorbed O_2 on the surface vacancies; the third peak at an even higher temperature stemmed from the lattice oxygen O_2^- species on the sample surface.[26–29] We normalized these two curves to be comparable in terms of the integrated area, and hence to be able to describe the total amount of oxygen stored. From the comparison, we noticed that the total amount of oxygen adsorbed for the aged sample was 2.46 fold less than that of the fresh sample.

Furthermore, we measured the BET surface areas to double check the effect of aging on the morphology of the sample. The fresh sample showed a decent surface area of 58.84 m^2 g^{-1}, which was reduced to 19.19 m^2 g^{-1} after aging the sample, *i.e.*, a 3.11-fold reduction. These results also showed the BET surface area and O_2-TPD to be strongly correlated.

Masses of 100 mg of the sieved fresh and aged $SmMn_2O_5$ samples were used to evaluate their catalytic performances with 450 ppm NO and 10% O_2 in the carrier gas N_2 at a total flow rate of 200 sccm. The percent conversion of NO to NO_2 in the presence of the fresh sample increased from about 5% to 90% as the temperature was increased form 50 °C to 275 °C, and then decreased as the temperature was increased further to 400 °C (Fig. 6a). In contrast, the aged sample displayed a lower peak percent conversion, with a value of ~80%, than did the fresh sample, and an approximately 25 °C higher light-off temperature. In addition, run tests of durability were also carried out at the conditions yielding the maximum NO conversion, respectively, for 16 h, as shown in Fig. 6b. The percent conversions of the fresh and aged samples were only reduced 2% and 4%, respectively, after 16 h.

In order to clarify the mechanism of the hydrothermal aging, we prepared pure phases of $SmMn_2O_5$, $SmMnO_3$ and Mn_2O_3 to determine the differences in their catalytic performances. Under the same conditions, $SmMn_2O_5$ and Mn_2O_3 were found to show similar behaviors at temperatures higher than 175 °C (Fig. 7) with a maximum conversion of 89% at 275 °C. And $SmMn_2O_5$ displayed slightly higher conversion than did Mn_2O_3 below 175 °C. In comparison, perovskite $SmMnO_3$ showed a relatively low NO oxidation activity of about 78%, and the light-off temperature increased by 50 °C. According to the mullite decomposition formula ($2SmMn_2O_5 \xrightarrow{\Delta} 2SmMnO_3 + Mn_2O_3 + O_2(g)$), the performance of the aged sample would be expected to decrease when the perovskite phase appears.

As seen in Table 1, and as described above, the BET area of the fresh sample was determined to be 58.84 m^2 g^{-1}, and that of the hydrothermally aged sample was 19.19 m^2 g^{-1}. The BET surface area of the fresh $SmMn_2O_5$ was comparable to those of $SmMnO_3$ and Mn_2O_3. The result of BET surface area clearly indicated that the aggregation of $SmMn_2O_5$ together with the formation of the new phases after hydrothermal aging led to the reduction of the BET surface area and the catalytic performance.

Conclusions

In summary, we systematically explored the influence of hydrothermal aging on the morphology of a mullite catalyst and on the performance of its catalysis of NO oxidation. XRD, HRTEM, XPS and Raman spectroscopy analyses together showed the appearance of new Mn_2O_3 and $SmMnO_3$ phases after hydrothermal treatment of the mullite sample. More importantly, the 110 nm-diameter rod-shaped particles of the fresh sample aggregated and increased in size to 200 nm upon being hydrothermally aged. The BET surface area of the aged sample was shown to be 2.46 times less than that of the fresh sample, consistent with O_2-TPD results. Tests of the separate phases including $SmMn_2O_5$, Mn_2O_3, and $SmMnO_3$ indicated a lower performance by perovskite $SmMnO_3$ than by the new Mn_2O_3 phase and mullite $SmMn_2O_5$. However, based on XRD and Raman spectra, the influence of the new phase on the mullite performance was limited due to the small relative amount of phase transition that occurred. Our work suggests that future work on the refinement of the mullite catalyst should focus on maintaining its surface area.

Conflicts of interest

The authors declare that they have no conflict of interests.

Acknowledgements

This work was supported by National Key Research and Development Program (Grant No. 2016YFB0901600), National Natural Science Foundation of China (21573117, and 11404172), the National Basic Research Program of China (973 Program with No. 2014CB931703).

References

1 W. Shan, F. Liu, Y. Yu, H. He, C. Deng and X. Zi, *Catal. Commun.*, 2015, **59**, 226–228.
2 Z. Fang, B. Yuan, T. Lin, H. Xu, Y. Cao, Z. Shi, M. Gong and Y. Chen, *Chem. Eng. Res. Des.*, 2015, **94**, 648–659.

3 B. Tu, W. Sun, Y. Xue, W. Q. Zaman, L. Cao and J. Yang, *ACS Sustainable Chem. Eng.*, 2017, **5**, 5200–5207.
4 M.-A. Tas, R. Van Hardeveld and E.-M. Van Veldhuizen, *Plasma Chem. Plasma Process.*, 1997, **17**, 4.
5 W. Wang, G. McCool, N. Kapur, G. Yuan, B. Shan, M. Nguyen, U.-M. Graham, B.-H. Davis, G. Jacobs, K. Cho and X. Hao, *Science*, 2012, **17**, 337.
6 Y. Xu, H. Liu, Z. Zhang and Y. Chen, *Chin. J. Environ. Eng.*, 2010, **4**(7), 1605–1608.
7 M. Kaneeda, H. Iizuka, T. Hiratsuka, N. Shinotsuka and M. Arai, *Appl. Catal., B*, 2009, **90**, 564–569.
8 H. Chang, G. Qi, K. Dahlberg and W. Li, *Science*, 2010, **327**, 1624–1627.
9 Y. Zhang, D. Wang, J. Wang, Q. Chen, Z. Zhang, X. Pan, Z. Miao, B. Zhang, Z. Wu and X. Yang, *Chin. J. Catal.*, 2012, **33**, 1448–1454.
10 Q. Zhang, Z. Song, P. Ning, X. Liu, H. Li and J. Gu, *Catal. Commun.*, 2015, **59**, 170–174.
11 J. Luo, F. Gao, K. Kamasamudram, N. Currier, C.-H.-F. Peden and A. Yezerets, *J. Catal.*, 2017, **348**, 291–299.
12 B. Pereda-Ayo, U. De La Torre, M. J. Illan-Gomez, A. Bueno-Lopez and J. Gonzalez-Velasco, *Appl. Catal., B*, 2014, **147**, 420–428.
13 P. Vennestrom, T. Janssens, A. Kustov, M. Grill, A. Puig-Molina, L. Lundegaard, R. Tiruvalam, P. Concepcion and A. Corma, *J. Catal.*, 2014, **309**, 477–490.
14 Y. Chen, H. Yuan, G. Li, G. Tian and S. Feng, *J. Cryst. Growth*, 2007, **305**, 242–248.
15 X. Wang, G. Li, Q. Chu, X. Liu and S. Feng, *Chem. J. Chin. Univ.*, 2007, **28**, 821–823.
16 A.-M. Yankin, O.-M. Fedorova, V.-F. Balakirev and Y.-V. Golikov, *Russ. J. Phys. Chem.*, 2007, **81**, 139–142.
17 H. Li, Z. Yang, J. Liu, X. Yao, K. Xiong, H. Liu, W. H. Wang and W. Wang, *Appl. Phys. Lett.*, 2016, **109**, 211903.
18 J. Liu, M. Yu, X. Wang, J. Wu, C. Wang, L. Zheng, D. Yang, H. Liu, Y. Yao, F. Lu and W. Wang, *J. Mater. Chem. A*, 2017, **5**, 20922.
19 C. Lu, J. Fan, H. Liu, K. Xia, K. Wang, P. Wang, Q. He, D. Yu and J. Liu, *Appl. Phys. A*, 2009, **96**, 991–996.
20 W.-R. Wang, D.-P. Xu and W.-H. Su, *Chin. Phys. Lett.*, 2005, **22**, 3.
21 S.-H. Shim, D. LaBounty and T.-S. Duffy, *Phys. Chem. Miner.*, 2011, **38**, 685–691.
22 J. Xu, Y. Deng, Y. Luo, W. Mao, X. Yang and Y. Han, *J. Catal.*, 2013, **300**, 225–234.
23 P.-M. Csernica, J.-R. McKone, C.-R. Mulzer, W.-R. Dichtel, H.-D. Abruña and F.-J. DiSalvo, *ACS Catal.*, 2017, **7**, 3375–3383.
24 Y. Lou, J. Ma, W. Hu, Q. Dai, L. Wang, W. Zhan, Y. Guo, X. Cao, Y. Guo, P. Hu and G. Lu, *ACS Catal.*, 2016, **6**, 8127–8139.
25 C. Deng, Q. Huang, X. Zhu, Q. Hu, W. Su, J. Qian, L. Dong, B. Li, M. Fan and C. Liang, *Appl. Surf. Sci.*, 2016, **389**, 1033–1049.
26 J. Ma, G. Jin, J. Gao, Y. Li, L. Dong, M. Huang, Q. Huang and B. Li, *J. Mater. Chem.*, 2015, **3**, 24358–24370.
27 H. Cheng, N. Zhang, X. Xiong, X. Lu, H. Zhao, S. Li and Z. Zhou, *ACS Sustainable Chem. Eng.*, 2015, **3**, 1982–1992.
28 L. Dong, Y. Tang, B. Li, L. Zhou, F. Gong, H. He, B. Sun, C. Tang, F. Gao and L. Dong, *Appl. Catal., B*, 2016, **180**, 451–462.
29 C. Deng, B. Li, L. Dong, F. Zhang, M. Fan, G. Jin, J. Gao, L. Gao, F. Zhang and X. Zhou, *Phys. Chem. Chem. Phys.*, 2015, **17**, 16092.